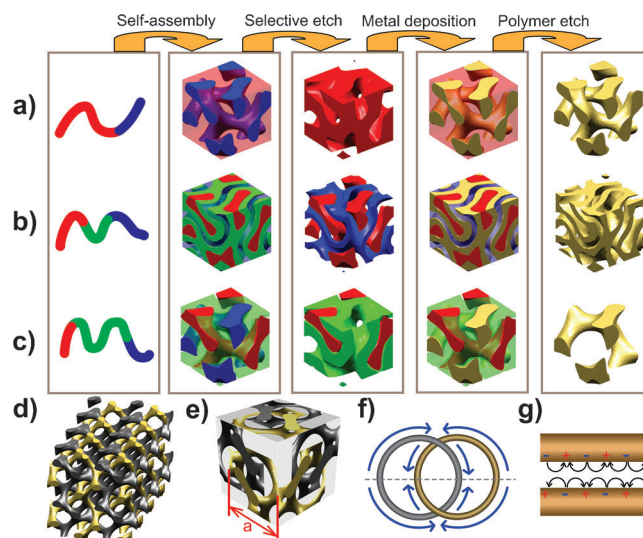


# Three-Dimensionally Isotropic Negative Refractive Index Materials from Block Copolymer Self-Assembled Chiral Gyroid Networks\*\*

Kahyun Hur, Yan Francescato, Vincenzo Giannini, Stefan A. Maier, Richard G. Hennig, and Ulrich Wiesner\*

In 1999, Pendry et al. predicted that specifically engineered artificial materials, that is, metamaterials, would have unusual magnetic responses, for example, negative permeability.<sup>[1]</sup> Following this work, much effort has been devoted to the design and fabrication of metamaterials with negative refractive index.<sup>[2,3]</sup> Such negative index metamaterials have the potential, for example, in the form of superlenses, to overcome the diffraction limit in imaging or to enable novel optical effects, including cloaking.<sup>[4]</sup> Today most metamaterial fabrication relies on top-down approaches such as lithography techniques, making efficient access to three-dimensionally (3D) isotropic metamaterials challenging thus hindering their practical applications.<sup>[5]</sup> Recent progress in bottom-up type self-assembly offers promise to overcome some of these limitations.<sup>[6]</sup> In particular block copolymer (BCP) self-assembly has emerged as a useful designer tool to create nanostructures including 3D continuous morphologies of disparate materials like ceramics and metals.<sup>[7]</sup> The present paper makes clear theoretical predictions for how to design 3D isotropic materials with negative refraction and circularly polarized light propagation from a class of block copolymer based self-assembled materials not yet rigorously studied in the context of metamaterials. Through theoretical understanding and guidance on materials choices, characteristic length and frequency scales, which are determined by calculations and described in detail here, a “recipe” is provided for the synthesis, fabrication and characterization of these materials.

We present calculations of the photonic properties of 3D periodic metallic nanomaterials with co-continuous cubic morphologies as illustrated in Figure 1. Such structures are



**Figure 1.** Schematic routes to 3-dimensionally co-continuous metamaterials with cubic symmetry and expected optical behavior. a) D-GYR; b) hollow D-GYR; and c) A-GYR metamaterials. For clarity of presentation, specific blocks are represented to be transparent. d) D-GYR metamaterial formed from many unit cells. The two chiral gyroid struts are depicted in different color for clarity. e) Projected images of a D-GYR metamaterial unit cell with unit cell length  $a$  onto three orthogonal axes. Two struts are cut in different planes for showing full loops. Surface plasmon polaritons f) oscillate on the closed loop of gyroid networks and g) on a 1-dimensional metal/insulator/metal wave-guide.

experimentally accessible through self-assembly of AB diblock copolymers and ABC triblock terpolymers and are referred to as double gyroid (D-GYR) and alternating gyroid (A-GYR). Both of these structures have two 3D continuous cubic and interwoven minority networks separated by a matrix majority network. In the A-GYR the two minority networks are distinguishable leading to chirality while in the D-GYR they are not. We predict for the resulting metallic nanomaterials that the coupled surface plasmon resonance of the two minority networks of the D-GYR induces low frequency light propagation with a negative index of refraction. Due to their cubic symmetry, these materials are 3D isotropic (see Figure 1 e). They also show circularly polarized light propagation originating from the chirality of the gyroid networks. We further predict that by tailoring BCP synthesis one can design materials with varying refractive index and frequency at which negative refraction occurs. Finally, in contrast to D-GYR metallic nanomaterials, chiral A-GYR metallic nanomaterials are expected to exhibit a surprising metallic band gap despite their smaller metallic fraction. We

[\*] K. Hur, Prof. R. G. Hennig, Prof. U. Wiesner  
 Department of Material Science and Engineering, Cornell University  
 Ithaca, NY, 14853 (USA)  
 E-mail: ubw1@cornell.edu

Y. Francescato, Dr. V. Giannini, Prof. S. A. Maier  
 Physics Department, Imperial College London  
 South Kensington, London SW7 2AZ (United Kingdom)

[\*\*] This publication is based on work supported in part by Award No. KUS-C1-018-02, made by King Abdullah University of Science and Technology (KAUST). The calculations have been performed using computational resources of the Computational Center for Nanotechnology Innovation (CCNI) at Rensselaer Polytechnic Institute. The work was further supported by the National Science Foundation through the Materials World Network grant between the US (DMR-1008125) and Great Britain (Engineering and Physical Sciences Research Council).

Supporting information for this article is available on the WWW under <http://dx.doi.org/10.1002/anie.201104888>.

conclude that these periodic structures would effectively behave like metamaterials.

A gyroid is a 3D co-continuous structure with cubic symmetry based on the triply periodic G minimal surface (see Figure 1 and Ref. [8] for their topological characteristics). Minimal surfaces have a mean curvature of zero everywhere. Familiar examples include surfaces of minimum area formed by soap films obtained from dipping wire frames into soap solutions. Due to characteristics of materials with cubic symmetry, metamaterials with gyroid structure are inherently isotropic in 3D and so are their optical responses<sup>[9]</sup> as compared to other metamaterials.<sup>[1,3]</sup> After the first discovery of a gyroid in BCP self-assembly, gyroid-based materials self-assembly has received significant attention and in the meantime has led to the first electronic devices.<sup>[10]</sup> Furthermore, such 3D isotropic gyroidal structures have also been found in intermetallic compounds.<sup>[11]</sup> The D-GYR morphology is composed of two minority networks of the same monomer species obtained from AB diblock copolymers, where each network has opposite chirality and is the inversion of the other. Due to this inversion symmetry, the structure is not chiral, and belongs to the space group  $Ia\bar{3}d$ , denoted  $Q^{230}$ .<sup>[12]</sup> In contrast, the A-GYR has two minority networks composed of different monomer species and is obtained from ABC triblock terpolymers (red and blue domains in Figure 1c). Since the two minority networks are chemically distinct the structure lacks inversion symmetry and becomes chiral with space group  $I4_132$ , denoted  $Q^{214}$ .<sup>[12]</sup> Our metamaterials are designed by assuming selective etches of different blocks of AB diblock and ABC triblock polymer derived gyroids and deposition of metal into the resulting pores as shown in the schematic diagrams in Figure 1. Recent synthetic progress<sup>[13]</sup> suggests that the proposed schemes are feasible for metamaterials fabrication.

Before describing the results of our calculations, it is instructive to look into what kind of optical behavior can be expected for the gyroid structures shown in Figure 1. It is expected that 3D continuous metallic networks have a metallic band gap below a certain cut-off frequency due to a strong plasmon response at low frequencies.<sup>[14]</sup> However, for the D-GYR morphology, the two separate gyroid networks form a capacitor leading to a different light propagation mechanism. Such light propagation originates from the coupled surface plasmon resonances on the closed loops of gyroid networks (see Figure 1d–f). The gyroid capacitor becomes a metal/insulator/metal (MIM) wave-guide as depicted in Figure 1g. This coaxial MIM geometry<sup>[15]</sup> supports surface plasmon polariton propagation. Resulting photonic behaviors are very unique. The longest wavelength at the Brillouin zone boundary reaches  $\lambda = 34a$  in vacuum for a D-GYR metamaterial with unit cell size,  $a = 25$  nm. Furthermore, as will be shown below, their refractive index and frequency range can be controlled by the lattice constant, that is, without changing the deposited materials. Due to limitations of the unit cell size to values typically below 150 nm,<sup>[16]</sup> dielectric materials-based photonic applications utilizing BCP self-assembly for visible and longer wavelengths are usually challenging.<sup>[17]</sup> However, the wave-guide bands result in negative refraction in visible and near-infrared regimes.

With calculations described below we confirm that in these bands the wave vector and the Poynting vector have opposite directions. Remarkably, these bands exhibit very small refractive index dispersion and propagation with low losses as shown in Figure S3b in the Supporting Information. Our theoretical results suggest that metamaterials fabrication from bottom-up BCP self-assembly may result in interesting optical properties thus moving them closer to the realm of practical applications.

We used self-consistent field theory, one of the most powerful methods to describe BCP morphologies,<sup>[18]</sup> to obtain realistic representations of the D-GYR and A-GYR morphologies. We subsequently calculated the photonic band structures of three different types of metal structures as shown in Figure 1, which we refer to as D-GYR, hollow D-GYR, and A-GYR metamaterials. For the calculations, two simulation methodologies were used, an eigensolver of Maxwell's equation following Ref. [19] and finite element-based software COMSOL.<sup>[20]</sup>

First, using the eigensolver approach, we calculated the band structures of the D-GYR metamaterial made of gold described by a Drude model<sup>[21]</sup> without losses with unit cell size,  $a = 100$  nm, and the plasma frequency,  $\omega_p = 2\pi \times 2.19 \times 10^{15}$  Hz, as shown in Figure 2. The characteristic flat bands of metallic photonic crystals<sup>[19,22]</sup> are observed within a frequency range,  $0.22 < \omega a/2\pi c < 0.55$ , the orange region in the band structure (see Figure 2a). Those bands are not shown due to extremely dense populations in this regime (note that the spacing between neighboring bands is less than  $10^{12}$  Hz). Figure 2b details the low-frequency bands. Despite the high portion of metal, low-frequency light propagation is observed. Interestingly, negative refraction bands are found and examples are highlighted in red (fast propagation) and green (slow propagation) in Figure 2b. For such negative refraction bands, the photonic flux given by the Poynting vector<sup>[23]</sup> is opposite to the momentum vector,  $\mathbf{k}$ . Figure 2c and d show the directions of the time-averaged local Poynting vector  $\mathbf{S} = 1/2 \text{Re}[\mathbf{E} \times \mathbf{H}^*]$  for positive and negative refraction bands. Clearly, the direction of  $\mathbf{S}$  is opposite to that of  $\mathbf{k}$  for negative refraction. Such negative refraction is further observed at different momentum vectors,  $\mathbf{k} = [0.1, 0.1, 0]$  and  $\mathbf{k} = [0.1, 0.1, 0.1]$ , as shown in Figure S1. Consequently, the photonic band is an all-angle negative refraction band. Since two interpenetrating networks form a metal/insulator/metal wave guide, such light propagation is allowed in D-GYR metamaterials. Figure 2e shows the polarization velocity field<sup>[19]</sup> of a positive refraction band (blue),  $\text{Re}[\mathbf{v}]$ , which corresponds to a coupled surface plasmon resonance. Each minority metal gyroid network has the anti-parallel electric currents of the other network and it is this coupled surface plasmon resonance phenomenon, which induces the propagation of light (see one cycle of  $\text{Re}[\mathbf{v}]$  shown in Movie S1 in the Supporting Information). Surprisingly, each chiral gyroid strut allows its own circular polarized light propagation (see Figure S2 and Movie S2).<sup>[24]</sup> Due to the existence of two opposite chiral struts, both left and right-handed circular polarizations can exist in D-GYR metamaterials.

In order to determine the importance of losses, we first calculated the band structure of lossy D-GYR metamaterials

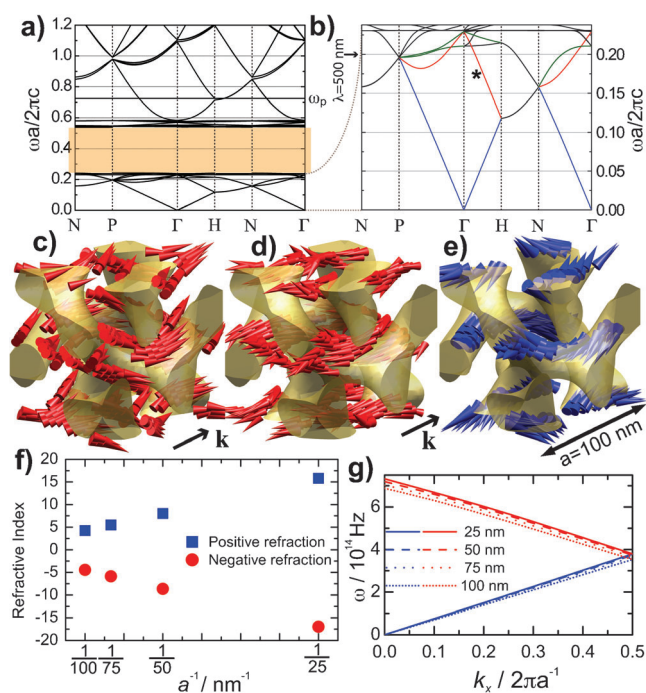


**Figure 2.** Results of band structure calculations using an eigensolver approach following Ref. [19] for D-GYR metamaterials made of a Drude metal with  $a = 100$  nm and the plasma frequency of gold,  $\omega_p = 2\pi \times 2.19 \times 10^{15}$  Hz.<sup>[21]</sup> a) Photonic band structure of D-GYR where the shaded region is filled with extremely dense flat bands. b) Expanded view for low-frequency bands. Results show low-frequency propagation bands including positive refraction (examples highlighted in blue) and negative refraction (examples highlighted in red for fast and in green for slow bands, respectively). c) Energy flux,  $\mathbf{S}$ , of the positive refraction band (blue) at  $\mathbf{k} = [0.1, 0, 0]$ . d)  $\mathbf{S}$  of the negative refraction band (asterisk) at  $\mathbf{k} = [0.1, 0, 0]$ . e) Coupled plasmon resonance,  $\text{Re}[\omega]$ , of the blue band at  $\mathbf{k} = [0.1, 0, 0]$ . f) Refractive indices of two propagation bands (blue and red in b) obtained from  $\Gamma$  to H are roughly inversely proportional to the unit cell size,  $a$ . g) The band structure with varying  $a$ . The first Brillouin zone boundary is defined at  $\Gamma = [0, 0, 0]$ , H =  $[0.5, 0, 0]$ , N =  $[0.5, 0.5, 0]$ , and P =  $[0.5, 0.5, 0.5]$ . All momentum vectors,  $\mathbf{k}$ , have the unit  $2\pi/a$ .

with a damping term,  $\Gamma = 2\pi \times 5.79 \times 10^{12}$  Hz, without consideration of inter-band transitions<sup>[21]</sup> in the eigensolver approach. The results are shown in Figure S3 and show no significant deviations from the case without losses (note that metallic loss neither affects the band structure nor the energy flux). Second, calculations were compared for the negative band indicated with an asterisk (\*) in Figure 2b using COMSOL<sup>[20]</sup> for three different metals using experimental data of the dielectric function obtained from the literature: gold,<sup>[25]</sup> silver,<sup>[25]</sup> and aluminum.<sup>[26]</sup> As depicted in Figure 3a and b, metamaterials with silver and aluminum, respectively, show the same energy flux direction as the Drude metal case. In contrast, strong absorption from inter-band transitions in gold, which is not taken into account in the Drude model, prevents negative refraction to occur in that band (see Figure 3c). A strong frequency dispersion can change the direction of the group velocity.<sup>[27]</sup> Therefore, our calculations predict that low-loss metals like silver need to be employed in

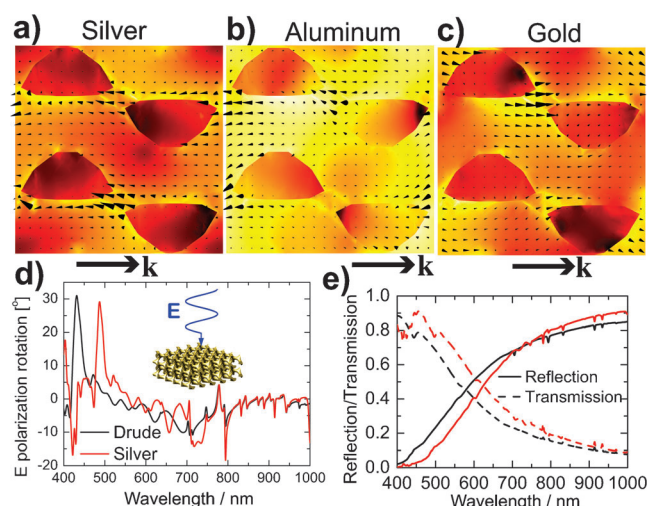


**Figure 3.** Results of finite element-based calculations using COMSOL. a–c) Normalized near-field profiles (yellow = 1, black = 0) and energy flux (arrows),  $\mathbf{S}$ , of the negative band indicated with an asterisk in Figure 2b at  $\mathbf{k} = [0.1, 0, 0]$  for different metals (dielectric function from experimental data): a) silver, b) aluminum, and c) gold. Silver and aluminum show the same directional behavior of  $\mathbf{S}$  calculated for gold in the Drude model (in which inter-band losses are not considered), while the direction of  $\mathbf{S}$  in gold is positive due to strong losses from inter-band transitions. d) Far-field simulation results of a A-GYR slab composed of two unit cells with  $a = 100$  nm demonstrate electric field polarization rotation angle for the Au Drude metal (black) and silver (red). e) Reflectance (solid lines) and transmittance (broken lines) of the slab.

the BCP self-assembly directed metamaterials described here to observe negative refraction in the visible range.

One advantage of BCP self-assembly is a facile control of the unit cell size,  $a$ , which can be achieved by changing BCP molar mass. For BCP D-GYR morphologies  $a$  typically ranges from 25 nm to 150 nm.<sup>[16]</sup> We calculated the refractive index of a positive refraction (blue in Figure 2b) and a negative refraction (red) band for different unit cell sizes (see Figure 2f). The band structures are shown in Figure 2g with varying  $a$ . Interestingly, the frequency range for the negative refraction barely changes with  $a$ . This result implies that decreasing the gap between the gyroid metal networks linearly increases the wave vector  $\mathbf{k}$  at a fixed frequency. Physically, stronger coupling between surface plasmon resonances, that is, larger capacitance, induces slower surface plasmon polariton propagation as in 1-dimensional metal/insulator/metal waveguides.<sup>[15]</sup> This phenomenon sets metallic D-GYR metamaterials apart from their dielectric photonic crystal counterparts, where the band frequencies scale with  $a$  and the refractive indices are independent of  $a$ .<sup>[17,28]</sup> The results in Figure 2f and g show that for the D-GYR metamaterials the refractive index is roughly inversely proportional to  $a$ . Therefore, the refractive index of both positive and negative refraction bands can be controlled through tuning BCP molar mass. Such phenomena originate from the characteristics of the surface plasmon resonances. For this reason, controlling the surface plasmon resonance should be a critical design factor for band structure control at low frequencies.

One can expect that the surface plasmon resonance frequency of D-GYR metamaterials can be governed by the capacitance of the two minority networks. A larger capacitance may lower the frequency range of the negative refraction band by slowing surface plasmon polariton propagation. Intuitively, a smaller gap between the gyroid minority networks is expected to increase the capacitance. One possible block copolymer structure to achieve this is the so-called core-shell D-GYR observed in triblock terpolymers,<sup>[29]</sup> where the shells surrounding the two equivalent gyroid minority networks (cores) will be replaced by metals. Instead, in the current work, we assumed a conformal metal deposition on both D-GYR minority networks after removal of the majority (matrix) block to ensure a shorter distance between two (hollow) metallic networks. The resulting hollow D-GYR metamaterial shown in the inset of Figure 4a has a smaller metal volume fraction of 0.11, as compared to 0.34 for the original structure. Figure 4a shows its band structure for a unit cell size  $a = 100$  nm. As expected, negative refraction bands are observed in a lower frequency range (compare Figure 2b and Figure 4a).

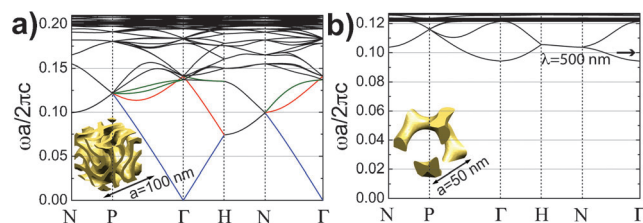


**Figure 4.** a) The photonic band structure of a hollow D-GYR metamaterial with  $a = 100$  nm shows a lower onset frequency of the negative refraction than D-GYR metamaterials (compare with results in Figure 2b). The color code is the same as in Figure 2. b) The metallic band gap of an A-GYR metamaterial with  $a = 50$  nm is observed in the photonic band structure up to  $\omega a/2\pi c = 0.094$ . The low-frequency propagation bands are missing due to lack of a “counter electrode”.

Finally, we calculated the band structure of A-GYR metamaterials with  $a = 50$  nm, where only one minority network is converted into a metal as shown in the inset of Figure 4b (note that for the same BCP molar mass, the unit cell size,  $a$ , of the A-GYR is approximately half the value of the D-GYR). Surprisingly, despite a much lower metallic volume fraction of 0.17, than that of the D-GYR of 0.34, such materials exhibit a metallic band gap at low frequencies.<sup>[30]</sup> Due to the lack of a “counter electrode”, low-frequency light propagation from the coupled surface plasmon resonance observed in the D-GYRs becomes forbidden. In order to see far-field effects, further calculations were performed using COMSOL for an A-GYR slab composed of two unit cells with  $a = 100$  nm for gold Drude metal and silver (note that this unit cell is twice as large as the one in Figure 4b). The results of the COMSOL calculations in Figure 3d show a broad peak of electric field polarization rotation below  $\lambda = 500$  nm, the frequency range of which coincides with the optically active range of the A-GYR band structure (losses in silver shift the peak and transmission/reflection spectra to longer wavelength as shown Figure 3d and e). Furthermore,

as expected in the D-GYR case, the chiral gyroid network in the A-GYR metamaterial induces a circular polarization (see the full cycle of  $\text{Re}[\mathbf{H}\mathbf{e}^{i\theta}]$  in Movie S3).

In summary, we calculated the photonic bands of 3D periodic metallic nanomaterials with D-GYR and A-GYR morphologies, which experimentally can be fabricated, for example, by using block copolymer self-assembly followed by selective etching and subsequent metal deposition. For the D-GYR structure, negative refraction is predicted in the visible and near-infrared regime for low-loss metals like silver and aluminum but not for gold. Due to the chirality of the gyroid minority networks, circularly polarized light propagation is predicted. We show that the refractive index and negative refraction frequencies of the resulting metamaterials are controlled by the structural parameters of these morphologies. For the A-GYR a surprising metallic band gap is observed at low frequencies. Cubic bicontinuous block copolymer network structures often have grain sizes of up to hundred micrometers or larger providing access to single-crystal type structures for which the phenomena described here should be measurable.<sup>[31]</sup>

Received: July 13, 2011

Revised: September 5, 2011

Published online: October 17, 2011

**Keywords:** metamaterials · nanomaterials · optics · polymers · self-assembly

- [1] J. B. Pendry, A. J. Holden, D. J. Robbins, W. J. Stewart, *IEEE Trans. Microwave Theory Tech.* **1999**, *47*, 2075–2084.
- [2] D. R. Smith, W. J. Padilla, D. C. Vier, S. C. Nemat-Nasser, S. Schultz, *Phys. Rev. Lett.* **2000**, *84*, 4184; R. A. Shelby, D. R. Smith, S. Schultz, *Science* **2001**, *292*, 77–79; E. Verhagen, R. de Waele, L. Kuipers, A. Polman, *Phys. Rev. Lett.* **2010**, *105*, 223901; N. Liu, H. Giessen, *Angew. Chem. Int. Ed.* **2010**, *49*, 9838–9852.
- [3] S. P. Burgos, R. de Waele, A. Polman, H. A. Atwater, *Nat. Mater.* **2010**, *9*, 407–412.
- [4] V. G. Veselago, *Sov. Phys. Usp.* **1968**, *10*, 509; J. B. Pendry, *Phys. Rev. Lett.* **2000**, *85*, 3966; J. B. Pendry, D. Schurig, D. R. Smith, *Science* **2006**, *312*, 1780–1782.
- [5] N. Liu, H. Guo, L. Fu, S. Kaiser, H. Schweizer, H. Giessen, *Nat. Mater.* **2008**, *7*, 31–37; M. S. Rill, C. Plet, M. Thiel, I. Staude, G. von Freymann, S. Linden, M. Wegener, *Nat. Mater.* **2008**, *7*, 543–546.
- [6] K. J. Stebe, E. Lewandowski, M. Ghosh, *Science* **2009**, *325*, 159–160; N. I. Zheludev, *Science* **2010**, *328*, 582–583; Q. Liu, Y. Cui, D. Gardner, X. Li, S. He, I. I. Smalyukh, *Nano Lett.* **2010**, *10*, 1347–1353.
- [7] S. C. Warren, L. C. Messina, L. S. Slaughter, M. Kamperman, Q. Zhou, S. M. Gruner, F. J. DiSalvo, U. Wiesner, *Science* **2008**, *320*, 1748–1752; “Bioinspired Block Copolymer-Based Hybrid Materials”: M. Kamperman, U. Wiesner in *The Supramolecular Chemistry of Organic–Inorganic Hybrid Materials*, Wiley, Hoboken, **2010**.
- [8] A. H. Schoen, *Infinite Periodic Minimal Surfaces Without Self-Intersections*, National Aeronautics and Space Administration [for sale by the Clearinghouse for Federal Scientific and Technical Information, Springfield, Va.], Washington, **1970**; S. Leoni, I. A. Baburin, *Z. Kristallogr.* **2011**, *226*, 678–683.

- [9] R. E. Newnham, *Properties of Materials: Anisotropy, Symmetry, Structure*, Oxford University Press, Oxford, **2005**.
- [10] D. A. Hajduk, P. E. Harper, S. M. Gruner, C. C. Honeker, G. Kim, E. L. Thomas, L. J. Fetters, *Macromolecules* **1994**, *27*, 4063–4075; V. Z.-H. Chan, J. Hoffman, V. Y. Lee, H. Iatrou, A. Aygeropoulos, N. Hadjichristidis, R. D. Miller, E. L. Thomas, *Science* **1999**, *286*, 1716–1719; B.-K. Cho, A. Jain, S. M. Gruner, U. Wiesner, *Science* **2004**, *305*, 1598–1601; E. J. W. Crossland, M. Kamperman, M. Nedelcu, C. Ducati, U. Wiesner, D. M. Smilgies, G. E. S. Toombes, M. A. Hillmyer, S. Ludwigs, U. Steiner, H. J. Snaith, *Nano Lett.* **2009**, *9*, 2807–2812.
- [11] Y. Grin, U. Wedig, H. G. von Schnering, *Angew. Chem.* **1995**, *107*, 1318–1320; *Angew. Chem. Int. Ed. Engl.* **1995**, *34*, 1204–1206; R. Pöttgen, V. Hluchyy, A. Baranov, Y. Grin, *Inorg. Chem.* **2008**, *47*, 6051–6055.
- [12] T. Hahn, H. Wondratschek, U. Müller in *International Tables for Crystallography*, 5th ed. (International Union of Crystallography), Kluwer, Dordrecht, **2002**.
- [13] H.-Y. Hsueh, Y.-C. Huang, R.-M. Ho, C.-H. Lai, T. Makida, H. Hasegawa, *Adv. Mater.* **2011**, *23*, 3041–3046; A. Radke, T. Gissibl, T. Klotzbücher, P. V. Braun, H. Giessen, *Adv. Mater.* **2011**, *23*, 3018–3021.
- [14] M. M. Sigalas, C. T. Chan, K. M. Ho, C. M. Soukoulis, *Phys. Rev. B* **1995**, *52*, 11744.
- [15] B. Prade, J. Y. Vinet, A. Mysyrowicz, *Phys. Rev. B* **1991**, *44*, 13556.
- [16] A. J. Meuler, M. A. Hillmyer, F. S. Bates, *Macromolecules* **2009**, *42*, 7221–7250.
- [17] M. Maldovan, A. M. Urbas, N. Yufa, W. C. Carter, E. L. Thomas, *Phys. Rev. B* **2002**, *65*, 165123.
- [18] M. W. Matsen, M. Schick, *Phys. Rev. Lett.* **1994**, *72*, 2660; K. Hur, R. G. Hennig, F. A. Escobedo, U. Wiesner, *J. Chem. Phys.* **2010**, *133*, 194108–194112.
- [19] A. Raman, S. Fan, *Phys. Rev. Lett.* **2010**, *104*, 087401.
- [20] <http://www.comsol.com>.
- [21] M. A. Ordal, L. L. Long, R. J. Bell, S. E. Bell, R. R. Bell, J. R. W. Alexander, C. A. Ward, *Appl. Opt.* **1983**, *22*, 1099–1119.
- [22] J. B. Pendry, *J. Phys. Condens. Matter* **1996**, *8*, 1085.
- [23] J. D. Jackson, *Classical Electrodynamics*, 3rd ed., Wiley, New York, **1999**.
- [24] J. K. Gansel, M. Thiel, M. S. Rill, M. Decker, K. Bade, V. Saile, G. von Freymann, S. Linden, M. Wegener, *Science* **2009**, *325*, 1513–1515.
- [25] P. B. Johnson, R. W. Christy, *Phys. Rev. B* **1972**, *6*, 4370.
- [26] A. D. Raki, *Appl. Opt.* **1995**, *34*, 4755–4767.
- [27] G. Dolling, C. Enkrich, M. Wegener, C. M. Soukoulis, S. Linden, *Science* **2006**, *312*, 892–894.
- [28] J. D. Joannopoulos, *Photonic Crystals: Molding the Flow of Light*, 2nd ed., Princeton University Press, Princeton, **2008**.
- [29] C. A. Tyler, J. Qin, F. S. Bates, D. C. Morse, *Macromolecules* **2007**, *40*, 4654–4668.
- [30] V. Kuzmiak, A. A. Maradudin, F. Pincemin, *Phys. Rev. B* **1994**, *50*, 16835.
- [31] A. C. Finnefrock, R. Ulrich, A. Du Chesne, C. C. Honeker, K. Schumacher, K. K. Unger, S. M. Gruner, U. Wiesner, *Angew. Chem.* **2001**, *113*, 1247–1251; *Angew. Chem. Int. Ed.* **2001**, *40*, 1207–1211; A. C. Finnefrock, R. Ulrich, G. E. S. Toombes, S. M. Gruner, U. Wiesner, *J. Am. Chem. Soc.* **2003**, *125*, 13084–13093.